

A Helical-Deflector-Based Radio-Frequency Spiral Scanning System for keV Energy Electrons

Vanik Kakoyan^a, Simon Zhamkochyan^{a,*}, Vardan Bardakhchyan^a, Sergey Abrahamyan^a, Amur Margaryan^a, Aram Kakoyan^a, Hasmik Rostomyan^a, Anna Safaryan^a, Gagik Sughray^a, Hayk Gevorgyan^a, Artashes Paryan^a, Martin Pinamyan^a, Mikael Ivanyan^b, Satoshi N. Nakamura^c, John Annand^d, Kenneth Livingston^d, Rachel Montgomery^d, Patrick Achenbach^e, Josef Pochodzalla^e, Dimiter L. Balabanski^f, Ani Aprahamian^g, Viatcheslav Sharyy^h, Dominique Yvon^h, Hayk Elbakyan^a

^a*A.I. Alikhanyan National Science Laboratory (Yerevan Physics Institute), Yerevan, Armenia*

^b*CANDLE Synchrotron Research Institute, Yerevan, Armenia*

^c*Department of Physics, Graduate School of Science, the University of Tokyo, Tokyo, Japan*

^d*School of Physics and Astronomy, University of Glasgow, Glasgow, G12 8QQ, UK*

^e*Institut für Kernphysik, Johannes Gutenberg-Universität Mainz, Mainz, Germany*

^f*Extreme Light Infrastructure- Nuclear Physics (ELI-NP), Bucharest-Magurele, Romania*

^g*Department of Physics and Astronomy, University of Notre Dame, Notre Dame, IN 46556, USA*

^h*Département de Physique des Particules Centre de Saclay,*

Abstract

We present the design, modeling, and experimental validation of a radio-frequency based time-to-position conversion system for keV electrons incorporating a helical deflector operating in the 400-1000 MHz range. The device performs circular deflection of the electrons when driven by a single RF frequency and enables spiral scanning when two phase-locked RF voltages with slightly different frequencies are applied. The superposition of the two phase-locked RF voltages produces an amplitude-beating field whose slowly varying envelope modulates the deflection radius, transforming the circular scan into a controlled spiral on the detector plane. A detailed theoretical

*Corresponding author

Email address: szh@yerphi.am (Simon Zhamkochyan)

model describing the electron dynamics under two phase-locked RF voltages with different frequencies was derived, yielding analytical expressions for the transverse velocity and radius-vector components at the deflector exit. Spiral scanning will allow measurements with picosecond resolution in a time range 1-2 orders of magnitude larger than the period of the circular scanning.

Keywords: Radio-frequency photomultiplier tube; helical deflector; spiral scanning; keV energy electron; picosecond resolution;

1. Introduction

High-precision timing is indispensable in many disciplines, including particle and nuclear physics, astrophysics, ultrafast chemistry, biomedical imaging, and materials science. Here we report a development of a radio-frequency (RF) timer for keV-energy electrons based on a helical RF deflector operating in the 400-1000 MHz range [1, 2]. The deflector converts the arrival time of each electron into a position along a circular locus by performing continuous RF sweeps, enabling direct time-to-position mapping with low dead time. This concept is closely related to the RF photomultiplier tube (RFPMT) [3], which combines RF deflection with fast electron detection. Detection is performed using a microchannel plate (MCP) assembly coupled to a delay-line (DL) anode, which records the spatial distribution of impacts corresponding to the temporal structure of the incident electrons. Using an RF-synchronized femtosecond laser, a timing resolution of less than 10 ps has been demonstrated [2], limited mainly by the prototype geometry and operating frequency. The intrinsic dead time of the RFPMT is determined by the propagation time of signals in a DL anode, which are around 40 ns. The dead time can be significantly reduced by using a fast pixelated detector, such as Timepix4. Consequently, detection rates can be increased up to THz [4]. This would allow detection of multiple electron events separated by only a few picoseconds within a single scan cycle. The duration of one circular sweep corresponds to the inverse of the RF frequency: 2 ns at 500 MHz and 0.1 ns at 10 GHz. To extend the time range while maintaining ultrafast precision, we introduce a spiral-scanning technique employing two slightly different, phase-locked RF frequencies ω_1 and ω_2 [5, 6, 7]. The resulting pulsed image forms a slowly rotating spiral trajectory, increasing the duration of a single scan by several tens of times. The following sections present the theoretical background of the RF spiral-scanning system (Sec-

tion 2), experimental setup and results (Section 3), and concluding remarks (Section 4).

2. Theoretical Concept of the Spiral Scanning

The spiral-scanning principle is based on the beat phenomenon that arises from the superposition of two sinusoidal voltages with slightly different frequencies, f_1 and f_2 . The resulting electric field can be expressed as

$$E(t) = E_1(t) + E_2(t) = E_d \cos(2\pi f_1 t) + E_d \cos(2\pi f_2 t) = 2E_d \cos\left(2\pi \frac{f_1 - f_2}{2} t\right) \cos\left(2\pi \frac{f_1 + f_2}{2} t\right) \quad (1)$$

Here, $f_b = |f_1 - f_2|$ is the beat frequency, which determines the rate at which the amplitude envelope of the combined signal oscillates. For example, when $f_1 = 500$ MHz, $f_2 = 600$ MHz, and $E_d = 1$ V/m, a distinct beat pattern with $T_b = \frac{1}{f_b} = 10$ ns is observed, as shown in Fig. 1. For the case, when $f_1 = 500$ MHz and $f_2 = 505$ MHz the $T_b = 200$ ns.

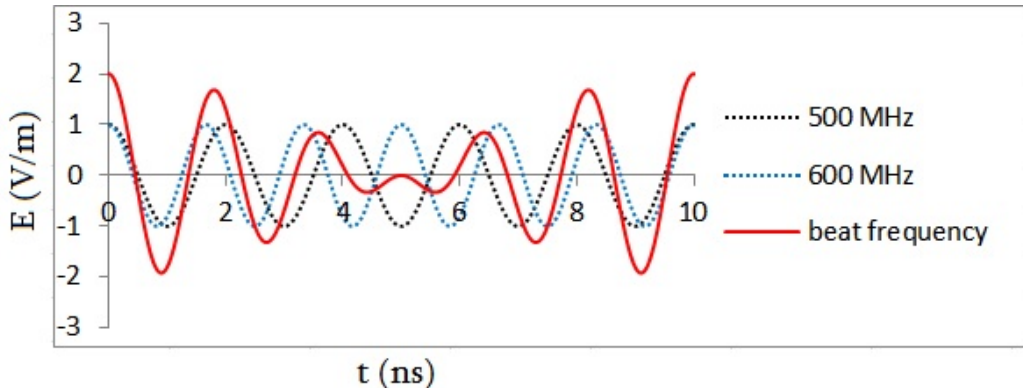


Figure 1: Beat phenomenon for frequencies of 500 MHz and 600 MHz.

In the previous study [1], a theoretical model of a helical deflector operating in the single frequency range of 400-1000 MHz was presented, along with experimental results. This deflector (Fig. 2), composed of two helical electrodes with a length L , separated by a distance d , was originally proposed for X-ray tubes to minimize transient-time effects at high frequencies.

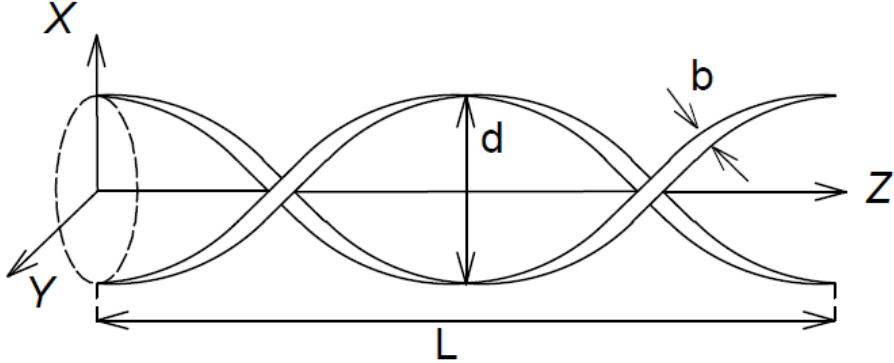


Figure 2: Schematic of the deflector.

Electrons enter the deflector along the Z-axis with a constant non-relativistic velocity V_z . For circular or elliptical scanning, the deflector is driven by an RF voltage of angular frequency ω_1 . As the electrons pass through the deflector, their transverse velocity components V_{x1} and V_{y1} at the end of the deflector are given by [1]:

$$V_{x1} = -\frac{eE_{d1}\tau}{2m_e} \left[\frac{\sin x_2}{x_2} \sin(x_2 + \varphi_1) - \frac{\sin x_1}{x_1} \sin(x_1 - \varphi_1) \right], \quad (2)$$

$$V_{y1} = -\frac{eE_{d1}\tau}{2m_e} \left[\frac{\sin x_1}{x_1} \cos(x_1 - \varphi_1) - \frac{\sin x_2}{x_2} \cos(x_2 + \varphi_1) \right]. \quad (3)$$

Where e and m_e are the charge and mass of the electron, respectively, E_{d1} and $\varphi_1 = \omega_1 t + \varphi_{01}$ are the amplitude and phase of the RF voltage, respectively, φ_{01} is the initial phase of the RF voltage at $t = 0$, and $\tau = L/V_z$ is the transit time of the electron through the deflector of length L . The parameters x_1 and x_2 are defined as

$$x_1 = \frac{\omega_c - \omega_1}{2}\tau, \quad x_2 = \frac{\omega_c + \omega_1}{2}\tau \quad (4)$$

where $\omega_c = (2\pi V_z)/\lambda_c$ is a parameter characterizing the deflector, with λ_c the winding pitch of the helical electrodes. We have circular (elliptical) scanning in the case of $\omega_1 = \omega_c$ ($\omega_1 \neq \omega_c$).

When two RF voltages with different angular frequencies ω_1 and ω_2 are applied to the deflector, the electron motion becomes the superposition of

two independent circular (elliptical) motions. The transverse velocity components at the end of the deflector in this case can be written as

$$V_x = V_{x1} + V_{x2} = -\frac{eE_{d1}\tau}{2m_e} \left[\frac{\sin x_2}{x_2} \sin(x_2 + \varphi_1) - \frac{\sin x_1}{x_1} \sin(x_1 - \varphi_1) \right] - \frac{eE_{d2}\tau}{2m_e} \left[\frac{\sin x'_2}{x'_2} \sin(x'_2 + \varphi_2) - \frac{\sin x'_1}{x'_1} \sin(x'_1 - \varphi_2) \right] \quad (5)$$

$$V_y = V_{y1} + V_{y2} = -\frac{eE_{d1}\tau}{2m_e} \left[\frac{\sin x_1}{x_1} \cos(x_1 - \varphi_1) - \frac{\sin x_2}{x_2} \cos(x_2 + \varphi_1) \right] - \frac{eE_{d2}\tau}{2m_e} \left[\frac{\sin x'_1}{x'_1} \cos(x'_1 - \varphi_2) - \frac{\sin x'_2}{x'_2} \cos(x'_2 + \varphi_2) \right] \quad (6)$$

where E_{d2} and φ_2 are the amplitude and phase of the second RF voltage, respectively, and the parameters x'_1 and x'_2 are related as

$$x'_1 = \frac{\omega_c - \omega_2}{2}\tau, \quad x'_2 = \frac{\omega_c + \omega_2}{2}\tau. \quad (7)$$

Introducing the parameters

$$k_1 = \frac{\omega_1}{\omega_c}, \quad k_2 = \frac{\omega_2}{\omega_c} \quad (8)$$

and considering equations (4)-(8), we obtain:

$$\begin{aligned} x_1 &= \frac{\omega_c - \omega_1}{2}\tau = (1 - k_1)\frac{\omega_c}{2}\tau = (1 - k_1)\pi \\ x_2 &= \frac{\omega_c + \omega_1}{2}\tau = (1 + k_1)\frac{\omega_c}{2}\tau = (1 + k_1)\pi \\ x'_1 &= \frac{\omega_c - \omega_2}{2}\tau = (1 - k_2)\frac{\omega_c}{2}\tau = (1 - k_2)\pi \\ x'_2 &= \frac{\omega_c + \omega_2}{2}\tau = (1 + k_2)\frac{\omega_c}{2}\tau = (1 + k_2)\pi \end{aligned} \quad (9)$$

The phase of the second voltage is expressed as $\varphi_2 = \omega_2 t + \varphi_{02}$, where φ_{02} is the initial phase of the second voltage at $t = 0$. Let's assume that the initial phase of first RF voltage is $\varphi_{01} = 0$ and that of the second RF voltage is $\varphi_{02} = \Delta\varphi$. Considering equation (8), we get:

$$\varphi_2 = \frac{k_2}{k_1}\varphi_1 + \Delta\varphi. \quad (10)$$

Substituting equations (9) and (10) into expressions (5) and (6), and replacing φ_1 with φ , we obtain:

$$\begin{aligned} \frac{V_x}{V_0} = & - \left[\frac{\sin(1+k_1)\pi}{(1+k_1)\pi} \sin((1+k_1)\pi + \varphi) \right. \\ & \left. - \frac{\sin(1-k_1)\pi}{(1-k_1)\pi} \sin((1-k_1)\pi - \varphi) \right] \\ & - a \left[\frac{\sin(1+k_2)\pi}{(1+k_2)\pi} \sin\left((1+k_2)\pi + \frac{k_2}{k_1}\varphi + \Delta\varphi\right) \right. \\ & \left. - \frac{\sin(1-k_2)\pi}{(1-k_2)\pi} \sin\left((1-k_2)\pi - \frac{k_2}{k_1}\varphi - \Delta\varphi\right) \right] \end{aligned} \quad (11)$$

$$\begin{aligned} \frac{V_y}{V_0} = & - \left[\frac{\sin(1-k_1)\pi}{(1-k_1)\pi} \cos((1-k_1)\pi - \varphi) \right. \\ & \left. - \frac{\sin(1+k_1)\pi}{(1+k_1)\pi} \cos((1+k_1)\pi + \varphi) \right] \\ & - a \left[\frac{\sin(1-k_2)\pi}{(1-k_2)\pi} \cos\left((1-k_2)\pi - \frac{k_2}{k_1}\varphi - \Delta\varphi\right) \right. \\ & \left. - \frac{\sin(1+k_2)\pi}{(1+k_2)\pi} \cos\left((1+k_2)\pi + \frac{k_2}{k_1}\varphi + \Delta\varphi\right) \right] \end{aligned} \quad (12)$$

where φ is the phase of the first RF, $a = E_{d2}/E_{d1}$ and $V_0 = eE_{d1}\tau/2m_e$ are constant parameters.

To find the transverse components of the electron's radius vector on the plane at the end of the deflector, we integrate equations (11) and (12) with respect to the phase time of the RF voltage over the interval from t to $t + \tau$, where t and $t + \tau$ are the times at which the electron enters and leaves the deflector, respectively, we get:

$$\begin{aligned}
\frac{r_x}{r_0} = & \frac{\sin(1+k_1)\pi}{(1+k_1)\pi} [\cos((1+k_1)\pi + \varphi + 2\pi k_1) - \cos((1+k_1)\pi + \varphi)] \\
& + \frac{\sin(1-k_1)\pi}{(1-k_1)\pi} [\cos((1-k_1)\pi - \varphi - 2\pi k_1) - \cos((1-k_1)\pi - \varphi)] \\
& + a \frac{k_1 \sin(1+k_2)\pi}{k_2 (1+k_2)\pi} \left[\cos\left((1+k_2)\pi + \frac{k_2}{k_1}\varphi + 2\pi k_2 + \Delta\varphi\right) \right. \\
& \quad \left. - \cos\left((1+k_2)\pi + \frac{k_2}{k_1}\varphi + \Delta\varphi\right) \right] \\
& + a \frac{k_1 \sin(1-k_2)\pi}{k_2 (1-k_2)\pi} \left[\cos\left((1-k_2)\pi - \frac{k_2}{k_1}\varphi - 2\pi k_2 - \Delta\varphi\right) \right. \\
& \quad \left. - \cos\left((1-k_2)\pi - \frac{k_2}{k_1}\varphi - \Delta\varphi\right) \right]
\end{aligned} \tag{13}$$

$$\begin{aligned}
\frac{r_y}{r_0} = & \frac{\sin(1+k_1)\pi}{(1+k_1)\pi} [\sin((1+k_1)\pi + \varphi + 2\pi k_1) - \sin((1+k_1)\pi + \varphi)] \\
& + \frac{\sin(1-k_1)\pi}{(1-k_1)\pi} [\sin((1-k_1)\pi - \varphi - 2\pi k_1) - \sin((1-k_1)\pi - \varphi)] \\
& + a \frac{k_1 \sin(1+k_2)\pi}{k_2 (1+k_2)\pi} \left[\sin\left((1+k_2)\pi + \frac{k_2}{k_1}\varphi + 2\pi k_2 + \Delta\varphi\right) \right. \\
& \quad \left. - \sin\left((1+k_2)\pi + \frac{k_2}{k_1}\varphi + \Delta\varphi\right) \right] \\
& + a \frac{k_1 \sin(1-k_2)\pi}{k_2 (1-k_2)\pi} \left[\sin\left((1-k_2)\pi - \frac{k_2}{k_1}\varphi - 2\pi k_2 - \Delta\varphi\right) \right. \\
& \quad \left. - \sin\left((1-k_2)\pi - \frac{k_2}{k_1}\varphi - \Delta\varphi\right) \right]
\end{aligned} \tag{14}$$

where $r_0 = eE_{d1}\tau^2/4k_1\pi m_e$.

As stated above, the theoretical analysis provides explicit expressions for the transverse components of the electron's radius vector, which determined by following parameters of the deflector:

1. a - the amplitude ratio of the two RF voltages;
2. $\Delta\varphi$ - the initial phase difference of the two RF voltages;
3. k_1 and k_2 which are defined by the f_1 , f_2 frequencies and the ω_c parameter of the helical deflector.

3. Experimental Studies

Experiments were performed using the setup schematically illustrated in Fig. 3. The system consists of several components: a UV photon source, an RF timer, an RF source, associated electronics, a data acquisition (DAQ) system, power supplies, and a vacuum chamber. The components of the RF timer [2] are assembled in a single tube and operated under a vacuum of 10^{-6} Torr or better.

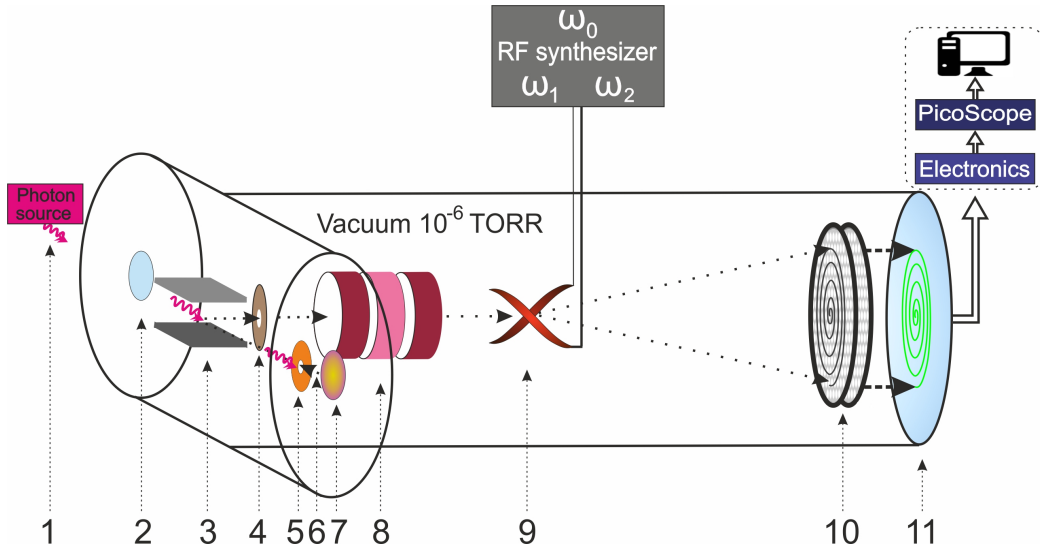


Figure 3: Schematic of the experimental setup. 1- UV photons; 2 - quartz window; 3 - magnet; 4 - collimator; 5 - accelerating electrode; 6 - photoelectron; 7 - cathode; 8 - electrostatic lens; 9 - RF deflector; 10 - MCP detector; 11 - delay line anode.

A 257 nm photons (1) from the light source were directed to the gold photocathode (7) to produce a continuous, low-energy electron beam (6). The electrons were accelerated by a 2.5 kV potential between the cathode (7) and an accelerating electrode (5), which was copper disk with a 1.5 mm central aperture positioned 3 mm from the cathode. The resulting beam was deflected by 90° using a permanent magnet (3) and collimated by a 0.7 mm aperture (4) before entering an electrostatic lens (8), which then focused the electrons onto the position sensitive detector (PSD).

The PSD consisted of a dual-chevron micro channel plate (MCP) (10) coupled to a delay-line (DL) anode (11). The MCP active area diameter was 25 mm. Before detection, the electrons passed through a helical RF deflector

(9) driven by an RF synthesizer. The RF deflector, located approximately 120 mm from the MCP, scanned ~ 2.5 keV electrons onto the MCP plane. Within the MCP, the electrons were multiplied by a factor of 10^6 and directed on to the DL anode, generating position-dependent signals with nanosecond rise times. Signal pairs were extracted through the vacuum flange, amplified by custom low-noise amplifiers, and digitized using PICOSCOPE hardware [8]. The electron hit position was reconstructed from the differences in arrival times of the signals from the delay line outputs.

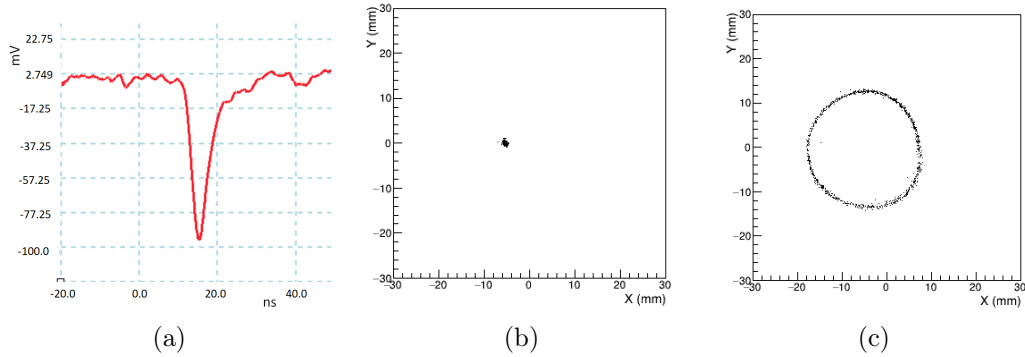


Figure 4: (a) typical amplified signals from the DL anode; (b) 2D image of the focused electrons (RF is OFF); (c) 2D image of the scanned electrons (500 MHz RF is ON).

Figure 4a shows the typical signal from the DL anode after amplification. When no RF is applied to the deflector, the image of the focused electrons on the anode is a dot (Fig. 4b), while an ellipse or circle is obtained (Fig. 4c) when RF is applied.



Figure 5: Photograph of the half-period deflector.

Experimental studies were performed using two different helical RF deflectors (half and full period), each having dimensions selected for a frequency of

500 MHz. A photograph of the first, half-period deflector is shown in Fig. 5. It is mounted in a quartz tube, has a diameter of 8 mm and a length of 30 mm.

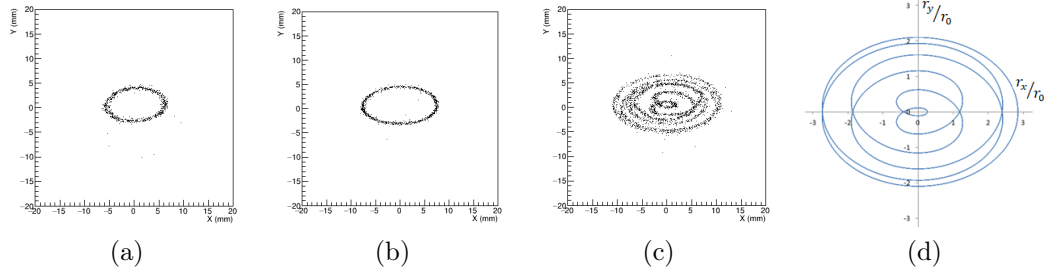


Figure 6: Half-period deflector: two-dimensional images of scanned electrons: (a) $f_1 = 500$ MHz, (b) $f_2 = 600$ MHz, (c) the combined frequencies $f_1 + f_2$ and (d) the corresponding theoretical image with $f_1 + f_2$, $f_c = 405$ MHz, $a = 1.23$ and $\Delta\varphi = \pi/2$. The dynamic range is $T_b = 10$ ns.

Subsequent measurements were performed using two different phase-locked RF frequencies. When only one RF signal was applied to the deflector the ellipse or circle was obtained on the anode. When two RF signals were applied, then a spiral was obtained. Figure 6 shows an example of experimental and theoretical results for two different RF signal parameters (see Section 2). The dynamic range of a single circular spectrum, which lasts about 2 ns at frequencies $f_1 = 500$ MHz or $f_2 = 600$ MHz, increases to $T_b = 10$ ns when two RF signals are applied together.

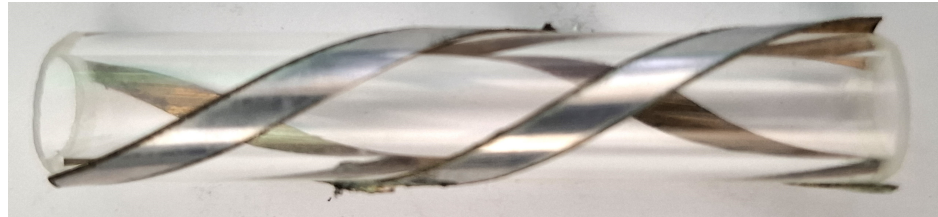


Figure 7: Photograph of the full period deflector.

Parameter $f_c = \omega_c/2\pi$ characterizes the deflector. In theory, f_c should be 500 MHz, but some deviation from this value is observed, which may be caused by non-uniform fields inside the deflector.

The second, full-period deflector was mounted on a quartz tube with a

diameter of 10 mm (see Fig. 7). It has a length of 60 mm. An example of the theoretical and experimental results for this deflector is shown in Fig. 8.

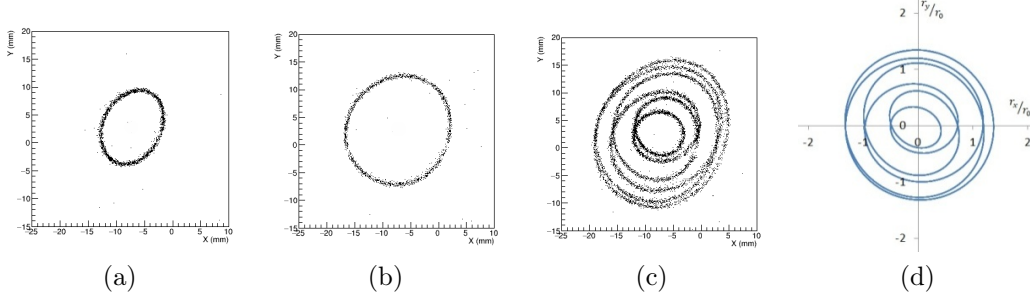


Figure 8: Two-dimensional images of scanned electrons: (a) $f_1 = 400$ MHz, (b) $f_2 = 480$ MHz, (c) the combined frequencies $f_1 + f_2$ and (d) the corresponding theoretical prediction with $f_c = 480$ MHz, $a = 1.66$ and $\Delta\varphi = 5\pi/9$. The dynamic range is $T_b = 12.5$ ns.

These results demonstrate that a deflector with a given set of parameters can operate efficiently over a relatively wide range of frequencies. Consequently, by using a deflector with suitable parameters, it becomes possible to achieve spiral scanning with a specified beat period in the needed frequency region throughout the 400–1000 MHz frequency range.

4. Conclusion

In this work, we report on the development and demonstration of a helical-deflector-based radio-frequency spiral scanning system capable of detecting keV energy electrons with a time resolution of a few picoseconds. A theoretical model describing the electron dynamics under two phase-locked RF voltages with different frequencies was derived, yielding analytical expressions for the transverse velocity and radius-vector components of electrons at the deflector exit. These expressions show that the resulting electron trace, and thus the time-to-position mapping, are fully determined by three fundamental parameters: the ratio of the RF amplitudes a , the initial phase offset $\Delta\varphi$, and the normalized frequencies k_1 and k_2 . The model predicts the formation of well-defined spiral traces whose shape and temporal scale can be precisely controlled through these parameters. Experimental measurements performed with 2.5 keV electrons confirm the theoretical predictions. Spiral

scans obtained using RF frequencies in the 400-1000 MHz range exhibit excellent agreement with simulations, validating both the helical-deflector concept and the two-frequency driving scheme. The spiral mode significantly extends the temporal range compared to conventional circular scanning, while retaining the underlying picosecond-level temporal resolution. The method provides high temporal precision, wide dynamic range, and compatibility with high-rate detection using MCP delay-line readout or next-generation pixel detectors. With further optimization, the approach offers a promising pathway toward very low dead-times and therefore, high-throughput timing devices for next-generation photodetectors.

Acknowledgments

This work was supported by the Higher Education and Science Committee of the Republic of Armenia (Research Project: 23LCG-1C018) and the International Science and Technology Center (ISTC project AM-2803).

References

- [1] L. Gevorgian, et al., A radio frequency helical deflector for kev electrons, Nuclear Instruments and Methods in Physics Research Section A 785 (2015) 175.
- [2] A. Margaryan, et al., An rf timer of electrons and photons with the potential to reach picosecond precision, Nuclear Instruments and Methods in Physics Research Section A 1038 (2022) 166926.
- [3] A. Margaryan, et al., Radiofrequency picosecond phototube, Nuclear Instruments and Methods in Physics Research Section A 566 (2006) 321.
- [4] A. Margaryan, et al., Single photon thz timer with radio frequency photomultiplier tube, in: Proceedings of PhotoDet2012, Orsay, France, 2012, poS PhotoDet2012 042.
- [5] S. M. Gurov, et al., Test of streak camera with high photoelectron beam density and energy, in: Proceedings of SPIE, Vol. 6279, 2007, p. 62790B.
- [6] J. F. M. van Rens, et al., Dual mode microwave detection cavities for ultrafast electron microscopy, Applied Physics Letters 113 (2018) 163104, arXiv:1901.09579.

- [7] H. Elbakyan, Helical deflecting system for streak cameras, Collection of Scientific Articles of YSU SSS 1.1 (11) (2016) 121.
- [8] Picotech, <https://www.picotech.com>.